Spatial heterogeneity in CO_2, CH_4, and energy fluxes: insights from airborne eddy covariance measurements over the Mid-Atlantic region

Reem A. Hannun[1,2], Glenn M. Wolfe[1,2], S. Randy Kawa[1], Thomas F. Hanisco[1], Paul A. Newman[1], Joseph G. Alfieri[3], John Barrick[4], Kenneth L. Clark[5], Joshua P. DiGangi[4], Glenn S. Diskin[4], John King[6], William P. Kustas[3], Bhaskar Mitra[7], Asko Noormets[7], John B. Nowak[4], K. Lee Thornhill[4], Rodrigo Vargas[8]

1. Atmospheric Chemistry and Dynamics Laboratory, NASA Goddard Space Flight Center, Greenbelt, MD, USA
2. Joint Center for Earth Systems Technology, University of Maryland Baltimore County, Baltimore, MD, USA
3. USDA Agricultural Research Service, Hydrology and Remote Sensing Laboratory, Beltsville, MD, USA
4. NASA Langley Research Center, Hampton, VA, USA
5. USDA Forest Service, Northern Research Station, Silas Little Experimental Forest, New Lisbon, NJ, USA
6. Department of Forestry and Environmental Resources, North Carolina State University, Raleigh, NC, USA
7. Department of Ecosystem Science and Management, Texas A&M University, College Station, TX, USA
8. Department of Plant and Soil Sciences, University of Delaware, Newark, DE, USA

Abstract

The exchange of carbon between the Earth's atmosphere and biosphere influences the atmospheric abundances of carbon dioxide (CO_2) and methane (CH_4). Airborne eddy covariance can quantify surface-atmosphere exchange from landscape-to-regional scales, offering a unique perspective on carbon cycle dynamics. We use extensive airborne measurements to quantify fluxes of sensible heat, latent heat, CO_2, and CH_4 across multiple ecosystems in the Mid-Atlantic region during September 2016 and May 2017. In conjunction with footprint analysis and land cover information, we use the airborne dataset to explore the effects of landscape heterogeneity on measured fluxes. Our results demonstrate large variability in CO_2 uptake over mixed agricultural and forested sites, with fluxes ranging from -3.4 ± 0.7 to -11.5 ± 1.6 μmol m^{-2} s^{-1} for croplands and -9.1 ± 1.5 to -22.7 ± 3.2 μmol m^{-2} s^{-1} for forests. We also report substantial

CH_4 emissions of 32.3 ± 17.0 to 76.1 ± 29.4 nmol m^{-2} s^{-1} from a brackish herbaceous wetland and 58.4 ± 12.0 to 181.2 ± 36.8 nmol m^{-2} s^{-1} from a freshwater forested wetland. Comparison of ecosystem-specific aircraft observations with measurements from eddy covariance flux towers along the flight path demonstrate that towers capture ~30–75% of the regional variability in ecosystem fluxes. Diel patterns measured at the tower sites suggest that peak, midday flux measurements from aircraft accurately predicts net daily CO_2 exchange. We discuss next steps in applying airborne observations to evaluate bottom-up flux models and improve understanding of the biophysical processes that drive carbon exchange from landscape-to-regional scales.

1 Introduction

The terrestrial biosphere plays a dynamic role in the global carbon cycle, removing an estimated 25–30% of the carbon dioxide (CO_2) emitted from fossil fuel emissions (Ciais *et al.*, 2013; Le Quéré *et al.*, 2018). However, the prognosis for this sink remains poorly constrained due to uncertain climate feedbacks on the atmosphere-biosphere cycling of CO_2 (Cox *et al.*, 2013; Wenzel *et al.*, 2016; Bond-Lamberty *et al.*, 2018). In addition, the land biosphere acts as a net source of methane (CH_4) (Saunois *et al.*, 2016; Tian *et al.*, 2016), with large uncertainties (>20 Tg/y) in magnitudes and ecosystem-dependent responses to climate state (Turner *et al.*, 2019). Thus, it is critical to accurately determine CO_2 and CH_4 fluxes, and their associated sensible and latent heat fluxes, from landscape-to-regional scales to better constrain the global carbon budget.

Several approaches exist for quantifying terrestrial carbon exchange. Top-down methods use a combination of observed atmospheric mixing ratios, transport models, and prior emissions estimates to infer fluxes of CO_2 (Houweling *et al.*, 2015; Wang *et al.*, 2018) and CH_4 (Bousquet *et al.*, 2011) on regional to global scales. These atmospheric inversion models provide a useful constraint on flux but offer limited attribution information on the underlying biophysical factors driving the carbon cycle. Bottom-up methods, in contrast, rely on biomass inventories (e.g. Pacala *et al.*, 2001; Pan *et al.*, 2011), surface flux tower networks (Baldocchi *et al.*, 2001; Jung *et al.*, 2011), or biophysical process models (e.g. Schaefer *et al.*, 2008) to extrapolate flux from local to global scales. However, inventory-based estimates have large associated uncertainties

of up to 75% (Hayes *et al.*, 2018), and discrepancies persist between different modeling approaches (Huntzinger *et al.*, 2012; Melton *et al.*, 2013) and model-tower data comparisons (Schwalm *et al.*, 2010; Schaefer *et al.*, 2012). Tower-based flux observations can provide benchmark information and a basis for validation, but their spatial representativeness is very limited at regional to continental scales (Villarreal *et al.*, 2018).

Airborne eddy covariance (EC) provides near-direct measurements of surface-atmosphere exchange over landscape-to-regional scales (e.g. Lenschow *et al.*, 1981; Desjardins *et al.*, 1982, 1989; Crawford *et al.*, 1996; Sellers *et al.*, 1997; Gioli *et al.*, 2004; Sayres *et al.*, 2017; Wolfe *et al.*, 2018). Such observations have successfully been used to evaluate CH_4 emissions inventories (Hiller *et al.*, 2014) and to scale up tower- or aircraft-based fluxes via empirically-derived environmental response functions (Miglietta *et al.*, 2007; Metzger *et al.*, 2013; Zulueta *et al.*, 2013). Airborne EC has also been applied to validate regional-scale flux inversions (Lauvaux *et al.*, 2009), light-use efficiency models of carbon and energy fluxes (Kustas *et al.*, 2006; Anderson *et al.*, 2008), and biophysical process models of forest carbon exchange (Maselli *et al.*, 2010).

Attribution of airborne fluxes requires knowledge of the spatial contribution of surface fluxes to the measurement at aircraft altitude: the flux footprint (Leclerc and Thurtell, 1990; Schuepp *et al.*, 1990). In conjunction with surface information (e.g. thematic land cover), footprint analysis enables the allocation of fluxes to the underlying surface state. For example, the flux fragment method (FFM) decomposes fluxes using the subset of observations that have a homogeneous footprint in the EC calculation (Kirby *et al.*, 2008; Dobosy *et al.*, 2017; Sayres *et al.*, 2017). While this method is highly reliable, it is best suited to regions with sufficient homogeneity to capture enough single-footprint observations, or to aircraft flying low enough to minimize the footprint size. More complex algorithms incorporate footprint-weighted land cover information to decompose observed fluxes using numerical or regression analysis (Chen *et al.*, 1999; Ogunjemiyo *et al.*, 2003; Wang *et al.*, 2006; Hutjes *et al.*, 2010). Such methods are more practical for data sets with mixed underlying terrain.

Here, we utilize an extensive airborne flux dataset to explore the effects of surface heterogeneity on the land-atmospheric exchange of sensible and latent energy, CO_2, and CH_4. Footprint analysis in conjunction with thematic land classification maps demonstrates that airborne fluxes can resolve spatial heterogeneity in land type at the 1–2 km^2 scale. We highlight campaign results for two case studies: a predominantly agricultural area between Maryland and Delaware, and a wetland forest located in coastal North Carolina. We further validate campaign measurements against flux observations from several towers and explore whether empirical time trends from towers yield a means of scaling airborne flux samples to net daily CO_2 exchange. Finally, we discuss next steps in utilizing airborne observations to calibrate and evaluate modeled flux products.

2 Methods

2.1 Airborne flux campaign and data

The NASA Carbon Airborne Flux Experiment (CARAFE) platform, payload, and data processing are described in detail by Wolfe et al. (2018). The data presented here were collected during two CARAFE deployments in September 2016 and May 2017. Flights spanned the Mid-Atlantic states and targeted a variety of land-use and ecosystem types, including forests, agricultural lands, and wetlands. Flux transects (Figure 1) cumulatively comprise ~7,000 km of linear distance, with typical altitudes of 80–300 m. Eddy covariance fluxes of sensible heat (H), latent heat (LE), CO_2 (F_{CO2}), and CH_4 (F_{CH4}) were determined via continuous wavelet transforms (Torrence and Compo, 1998), as detailed in Wolfe *et al.* (2018) and summarized in Section S1.1. 1-Hz processed flux data from the CARAFE campaigns, in addition to supporting scalar and winds data, are publicly available: https://www-air.larc.nasa.gov/missions/carafe/index.html.

2.2 Flux tower data

CARAFE flights included ~50 overpasses of flux towers (Figure 1). Table 1 lists key information for each tower. The USDA Choptank (USDA-Chop) tower is situated in the Choptank River watershed, an agricultural area of predominantly soy and corn crops on the eastern shore of the Chesapeake Bay (Sun *et al.*, 2017). The remaining four towers are part of the larger

AmeriFlux network. The St. Jones tower (US-StJ) samples the St. Jones Reserve tidal marsh in southeastern Delaware (Capooci *et al.*, 2019). The Cedar Bridge tower (US-Ced) and the Silas Little tower (US-Slt) are both located in the Pinelands National Reserve in southern New Jersey, with mostly pitch pine-dominated stands near US-Ced and mixed oak stands near US-Slt (Clark *et al.*, 2018). The US-NC4 tower is located in the Alligator River National Wildlife Refuge, a forested swamp in North Carolina (Miao *et al.*, 2017). Tower sites processed eddy covariance flux data according to standardized AmeriFlux procedures, as summarized in Section S1.2, and AmeriFlux data are publicly available: https://ameriflux.lbl.gov. All towers report H, LE, and F_{CO2}, while the US-StJ and US-NC4 locations additionally report F_{CH4}. With the inclusion of a small storage correction (typically <10%), towers also report net ecosystem exchange (NEE). Note that NEE is opposite in sign to F_{CO2}. The tower fetch across all sites ranges from 100–2500 m.

2.3 Flux decomposition by land class

2.3.1 Land classification

Land cover information was taken from the National Land Cover Database (NLCD 2016), a high-resolution (30 m x 30 m) map based on Landsat imagery (Yang *et al.*, 2018). The CARAFE domain includes 14 of the 20 NLCD land classes. Dominant land classifications sampled during CARAFE include woody wetlands (45%), cultivated crops (22%), and dry forests (evergreen, deciduous, and mixed classes) (21%). The remaining types are developed land (open, low, medium, and high density), open water, emergent herbaceous wetlands (hereafter herbaceous wetlands), shrubs, pastures, and grasslands, which individually make up less than 5% of the cumulative footprint.

2.3.2 2D flux footprint analysis

The flux footprint relates the spatial distribution of fluxes at the surface (F_s) to the observed flux (F_{obs}) measured at coordinates x_m, y_m and measurement height z_m (Horst and Weil, 1992; Schmid, 1994):

$$F_{obs}(x_m, y_m, z_m) = \iint_{-\infty}^{\infty} f(x, y, z_m) F_s(x, y, 0)\, dx\, dy \quad (1)$$

where, x and y are arbitrary horizontal coordinates and f is the flux footprint function, which expresses the contribution of each upwind unit surface element to F_{obs}. We use the two-dimensional Flux Footprint Prediction (2D-FFP) developed by Kljun *et al.* (2015), a parameterization based on a Lagrangian stochastic particle dispersion model (Kljun *et al.*, 2002) that is applicable to many turbulence regimes and measurement heights. The parameterization utilizes the following inputs: measurement height z_m, the mean horizontal wind speed U, the planetary boundary layer (PBL) height z_{bl}, the Obukhov length L_{OB}, the standard deviation of the lateral (crosswind) velocity fluctuations σ_v, and the friction velocity u^*. We derive σ_v from the wavelet variances of the horizontal wind velocity vectors.

We calculate the 2D-FFP for all 1 Hz data points (~75 m distance at typical flight speed) along all flux transects below 200 m. Each data point has an associated z_m, but leg-average values of the micro-meteorological variables (i.e. U, u^*, σ_v, L_{OB}) are used as the FFP is based on a mean flow parameterization, and point-to-point momentum fluxes exhibit significant variability. We estimate the boundary layer height from vertical profiles before and after each set of flux transects as described in Wolfe *et al.* (2018). Note that even a 20% error in z_{bl} has less than a 0.5% impact on the size and distribution of the footprint, except in highly stable conditions (Kljun *et al.*, 2015) atypical during the CARAFE flights. Once calculated, the 2D-FFP was rotated into the mean wind direction and transformed into the geographic coordinate space of the measurement, generating a gridded map of the footprint function associated with each flux observation. Figure 2 depicts an example of a single footprint for a flux measurement from the May 18, 2017 flight to Choptank, MD superimposed on the NLCD 2016 land cover map. For all flux observations from the 2016 and 2017 campaigns below 200 m in altitude, the 90% upwind extent for calculated footprints ranged from 1.5–10 km.

2.3.3 Disaggregation into component fluxes

To derive fluxes representative of a single land class, we use the Disaggregation combining Footprint analysis and Multivariate Regression (DFMR) methodology described by Hutjes *et al.* (2010). DFMR relies on the flux footprint and land cover to estimate a weighted contribution of

each land class to the flux measurement. The observed flux, F_{obs}, can be written as a linear summation of component fluxes from each of n land classes within the footprint:

$$F_{obs} = \sum_{k=1}^{n} C_k F_k \quad (2)$$

where C_k is the fractional area of the kth land class within the footprint and F_k is the corresponding component flux, or the mean land-class flux for a given set of observations (i.e., a single flight). The values C_k can be determined using the flux footprint function f to weight the relative contributions of land cover patches within the footprint, as patches closer to the sensor influence the measurement more heavily than patches farther away (Equations S1 and S2).

The multiple linear regression (Equation S3) was performed on a flight-by-flight basis to derive land-class component fluxes for each flight. A grid of 2D-FFP values was superimposed onto the NLCD 2016 map to generate the weighted fractional area of each land class in every footprint (see Figure 2). Although NLCD displayed 14 land classes in our sampling region, we down-selected for land classes that constituted more than 20% of the footprint-weighted area in at least 4 km of cumulative (but not necessarily consecutive) flux observations. This screening criterion, which was optimized via comparison with flux sub-samples from homogeneous footprints (Figure S1), ensured that selected land types were sampled enough to provide a meaningful average.

In addition to residual error, random and systematic measurement errors (see Wolfe *et al.*, 2018) were propagated through the regression, and errors were summed in quadrature to yield the total uncertainty for each component flux. Uncertainties in *a priori* surface characterization and footprint extent are not included. While the footprint calculation should introduce minimal error (barring significant changes to the fractional areas), mischaracterization of the surface cover could introduce significant biases. Corrections for vertical flux divergence are likewise not included due to large uncertainties in the correction factors (see Wolfe *et al.*, 2018). The flights all took place near midday and targeted fair-weather conditions. However, the data are not

screened for the presence of clouds, and such variations may contribute another source of flux variability in addition to those discussed below.

3 Results and Discussion

3.1 Disaggregated fluxes by region

3.1.1 Choptank watershed and St. Jones Reserve

CARAFE deployments included three flights to the Choptank agricultural area (September 12, 2016, May 4, 2017, and May 18, 2017). Flux transects spanned the Delmarva peninsula from the Chesapeake Bay to the Atlantic Ocean (typical length 60 km) and included overflights of the USDA-Chop and US-StJ towers (Figure 1). This region had mixed terrain, with six land classes meeting the down-selection criteria described in Section 2.3.3. Table 2 summarizes footprint-weighted contributions of each land class.

Disaggregated fluxes highlight the variability in carbon dynamics between land classes and over time (Figure 3). Of particular interest, cultivated crops (e.g., annual crops such as soybean or corn) and forested lands (e.g., woody wetlands and deciduous forest) display substantial differences in F_{CO2} for the sampling periods. The CO_2 uptake from cultivated crops ranged from -3.4 ± 0.7 to -11.5 ± 1.6 µmol m^{-2} s^{-1}, whereas deciduous and wetland forests display a much larger uptake, ranging from -12.1 ± 3.9 to -22.7 ± 3.9 µmol m^{-2} s^{-1} and -9.1 ± 1.5 to -22.7 ± 3.2 µmol m^{-2} s^{-1}, respectively. Forest uptake of CO_2 also dominates that by croplands in other regions with substantial cropland fraction (Fig. S2, S3). While the difference in CO_2 uptake between croplands and forest will be strongly dependent on crop type and phenology (Lokupitiya *et al.*, 2009), crops in the CARAFE region are typically in their early growth stages in May and undergoing senescence in September. Developed open lands, which comprise mostly lawn grasses and vegetation with < 20% impervious surface area, also draw down substantial CO_2 (~-13 to -30 µmol m^{-2} s^{-1}) during the May sampling period.

Choptank data also exhibit a general anticorrelation between F_{CO2} and LE, expected for vegetated land surfaces where transpiration and stomatal control is a major contributor to

evapotranspiration. The sampling is too limited to infer much about seasonal flux response for the various land types, but forested lands are comparably photosynthetically active during the growing season between May and September.

The disaggregation methodology also illustrates F_{CH4} variability with land type. F_{CH4} observations were at or below the detection limit for most CARAFE flights, and uncertainties are large due to poorly constrained regression results. However, it is known that soils from forested ecosystems represent a weak CH_4 sink (Subke *et al.*, 2018), whereas tree stems represent a weak CH_4 source (Vargas and Barba, 2019) that may counterbalance ecosystem scale CH_4 fluxes in upland forested ecosystems. In contrast, herbaceous wetlands, located primarily on the Eastern end of the track near the St. Jones tower, exhibit relatively strong CH_4 emissions of 76.1 ± 29.4 nmol m^{-2} s^{-1} on Sep-12 and 32.3 ± 17.0 nmol m^{-2} s^{-1} on May-04. This region has a mix of herbaceous wetlands that extend across a salinity gradient, where lower CH_4 emissions may be associated with wetlands in brackish waters and larger CH_4 emissions with freshwater wetlands (Poffenbarger *et al.*, 2011; Capooci *et al.*, 2019).

3.1.2 Alligator River

Three flights over the Alligator River region took place during the CARAFE deployments on September 24, 2016, May 15, 2017, and May 26, 2017. Flux transects spanned the Alligator River National Wildlife Refuge in the N-S direction, with the US-NC4 tower located near the middle of the flight transects (see Figure 1). The dominant land cover contributions included woody wetlands, open water, and some minor areas of cultivated crops and herbaceous wetlands. Table 2 contains a summary of the land-cover contributions to the footprint for Alligator River region.

The component fluxes from Alligator River display significant variability with land type (Figure 4). For example, the open water component of H is at or near zero for all flights, and evaporation dominates the surface energy fluxes for this class, as displayed by LE values generally greater than 200 W m^{-2}. Note that although classified as open water in the NLCD, the

coastal waters sampled near Choptank and Alligator River are actually comprised of estuarine waters and tidal mudflats. We observed occasional CO_2 emissions from these waters of 6.2 ± 2.2 µmol m^{-2} s^{-1} over the Alligator River (Sep-24, Fig. 4) and 6.4 ± 3.7 µmol m^{-2} s^{-1} in the Choptank region (May-18, Fig. 3). Both regions also display positive fluxes of CH_4, with means of 40.5 ± 12.2 nmol m^{-2} s^{-1} over the Alligator River and 20.5 ± 10.1 nmol m^{-2} s^{-1} in Choptank. These values are within the range of prior flux estimates, which can be up ~10 µmol CO_2 m^{-2} s^{-1} in low salinity estuarine waters, ~30-35 nmol CH_4 m^{-2} s^{-1} in tidal mudflats (Abril and Borges, 2005).

The woody wetlands land class, a freshwater forested swamp in the Alligator River region, also displays persistent, large CH_4 emissions ranging from 58.4 ± 12.0 to 181.2 ± 36.8 nmol m^{-2} s^{-1}. These unusually high values are recurrent and consistent over long periods at this site (Mitra *et al.*, 2019a), which has recorded among the highest CH_4 emissions from wetlands globally, including tropical wetlands. Other temperate swamplands exhibit mean CH_4 emissions of ~35 nmol m^{-2} s^{-1} (Turetsky *et al.*, 2014), but few global observational records exist for wetland ecosystems.

3.2 Comparison to tower flux observations

Direct comparison of aircraft and tower flux observations is challenging in heterogeneous landscapes, as the two platforms often sample different terrain due to the mismatch in footprint size (on the order of ~100 m for towers and ~3 km for CARAFE flights). During the CARAFE campaign, most flights contained numerous land cover types within a single footprint (Figure 2), resulting in an amalgamated signal from land-use and ecosystem states with varied carbon fluxes. In contrast, each tower sampled the local surface state with footprints that were typically homogeneous.

For each flight, tower data are averaged over the duration of the flight and compared to the aircraft disaggregated component flux corresponding to the tower's primary land class (Figure 5). Note that the aircraft component flux is derived using data from the entire flight region, and thus we are comparing a mean regional land-class flux to the site-specific land-class flux at the

tower location. The correlation between aircraft and tower fluxes varies between species, with H exhibiting the strongest correlation (r^2 = 0.76, Figure 5a) and the tightest fit (NRMSE = 15%). The slope of 0.58 ± 0.21 indicates a low bias in the aircraft fluxes, which may stem from the vertical flux divergence, which has not been included in the disaggregation. Divergence corrections typically range from ~10–60% with uncertainties of greater than 30% in the correction factors. LE fluxes display a slightly weaker correlation (r^2 = 0.53, Figure 5c) with notably more scatter between the aircraft and tower observations (NRMSE = 30%). F_{CO2} demonstrates similar scatter between the aircraft component fluxes and tower observations (NRMSE = 30%) but shows a weaker overall correlation (r^2 = 0.30) that may be skewed by a couple of outlying points in the US-Slt comparison (Figure 5b). The slopes for both LE (0.74 ± 0.31) and F_{CO2} (0.68 ± 0.31) contain substantial uncertainty in magnitude. The limited number of tower F_{CH4} observations make quantitative comparison with the aircraft fluxes difficult, and the correlation is not statistically significant, with a *p*-value > 0.05 (figure 5d). Nonetheless, aircraft data overrepresent CH_4 fluxes at US-StJ and underrepresent CH_4 fluxes at US-NC4.

Comparisons between the aircraft and tower observations suggest that local tower measurements capture 30–76% of the variance in regional ecosystem-dependent fluxes. The larger scatter (and weaker correlation) in observations of LE and F_{CO2} as compared to H could in part stem from errors in source area attribution. For example Kustas *et al.*, (2006) and Bertoldi *et al.*, (2013) found that footprint extents can differ between active (e.g., T) and passive scalars (e.g., H_2O, CO_2) in heterogeneous landscapes. A full quantification of the source contribution error requires computationally expensive boundary layer flow simulations outside the scope of this study.

Despite potential footprint inconsistencies, variability in the underlying drivers of carbon exchange within a land type expectedly results in discrepancies between aircraft and tower observations. In the Choptank watershed, where cultivated crops dominate the footprint, the disaggregation could be further refined based on crop type or land-use inventories to better quantify the effect of these parameters on CO_2 uptake (e.g., Zhang *et al.*, 2015). Additionally,

forested classes dominate several regions in the CARAFE domain, including the Alligator River and Pocomoke Forest (Table S2). Combining land cover with maps of forest canopy structure (Hurtt *et al.*, 2004) or metrics of photosynthetic activity, such as solar-induced fluorescence or vegetation indices (Frankenberg *et al.*, 2011), could provide additional observational constraints on the regional heterogeneity in the CO_2 sink.

In wetland regions, the underlying biogeochemical factors that control CH_4 emissions are not implicit with land class, and in some circumstances, CH_4 fluxes can be highly episodic and localized (Whalen, 2005). For example, CH_4 fluxes in the brackish herbaceous wetlands near the US-StJ site depend on flooding and drying conditions that change salinity gradients across the tidal zone (Capooci *et al.*, 2019). In the freshwater forested wetlands near US-NC4, Mitra *et al.*, (2019b) found that methanogen substrate availability produced via photosynthesis largely controls CH_4 flux, whereas water-table depth and surface temperature played a non-causal role in emissions. The complexity of the underlying controls of CH_4 fluxes stresses the need for continued regional-scale studies of these important yet understudied wetland ecosystems.

Although the observed variability in flux cannot be fully attributed to land class, the results emphasize the utility of spatially distributed observations in probing carbon cycle dynamics across heterogeneous regions. Typically, flux tower networks are used as ground-truth observations to evaluate carbon exchange in process models (Friend *et al.*, 2007; Raczka *et al.*, 2013) and to inform *a priori* errors in atmospheric inversions (Chevallier *et al.*, 2006). However, individual tower sites are limited in regional representativeness (this work; Villarreal *et al.*, 2018), and aircraft EC can provide a valuable supplement with which to examine landscape-scale changes in the underlying drivers of carbon exchange.

3.3 Upscaling with tower temporal trends

Tower flux observations offer a long-term record of local carbon cycle dynamics, of which aircraft observations only capture a brief subsample. Here, we explore whether the temporal

record of net ecosystem exchange (NEE) from towers can inform the extrapolation of local fluxes to regional, daily-integrated values using aircraft observations.

The tower sites included in the CARAFE domain demonstrate a distinct correlation between daily- and peak-NEE for the 2016 annual datasets (Figure S5). We define peak-NEE as the mean CO_2 exchange between 11:00 and 15:00 local, the time of day in which maximum CO_2 uptake by the biosphere is usually observed. Most CARAFE flights took place within this time frame. Daily-NEE is the 24-hour integral of half-hourly or hourly tower measurements. Figure 6a depicts the linear least squares fits of daily- versus peak-NEE for each individual tower site colored by land class, and the fit parameters and uncertainties are summarized Table 3. Note that this analysis does not account for inter-annual variability.

Four of the five tower sites display similar relationships between peak and daily exchange, with a mean slope of 0.30 ± 0.02, excluding US-StJ. The St. Jones tower samples a variable footprint, creating more scatter in the daily- vs. peak-NEE (see Figure S5, Table 3), and this site is strongly influenced by tides, which are known to affect diel patterns of NEE (Kathilankal *et al.*, 2008). Furthermore, mean diurnal NEE profiles for the month of August 2016 shown in Figure 6b reveal a larger ecosystem respiration from this land class as compared to other tower sites, accounting for the shallower slope of 0.21 ± 0.02. Nonetheless, the generally high correlations suggest that peak-NEE is predictive of net daily exchange across land types in the CARAFE domain, and peak CO_2 fluxes observed during the midday CARAFE flights encapsulate 50–90% of the day-to-day variability in carbon exchange. The temporal relationships observed at the tower sites thus provide a mechanism for inferring regional daily carbon exchange via airborne sampling.

Despite the similar relationships between daily- and peak-NEE across tower sites, ecosystem-dependent variability still results in large differences in carbon exchange, within and across individual days (e.g., Figures 3 and 4). A full assessment of the relationships between peak-NEE and longer-term trends is beyond the scope of this work. However, Zscheischler *et al.*, (2016)

have shown that observations of annual NEE from several tower sites in temperate forests, including US-Ced and US-Slt, demonstrate a strong correlation with the number of days having ecosystem fluxes above a high percentile. These analyses indicate that such temporal relationships can provide an empirical proxy for the climatic factors driving longer-term variability in carbon exchange. Furthermore, extracting longer-term information from airborne fluxes can facilitate comparison with flux inversions and process models, which often lack fine-timescale resolution.

4 Conclusions

We demonstrate that airborne fluxes, when combined with footprint and land cover information, resolve spatial heterogeneity in landscape flux. During the September and May sampling periods, results often show substantial differences in F_{CO2} with land type, and forests typically display a larger CO_2 uptake than croplands. This likely stems from the fact that in May most crops are typically still in early development and by September they are undergoing senescence heading towards harvest, whereas forests are consistently photosynthetically active during this time frame. We also observe a small but significant source of CH_4 from estuarine waters and tidal mudflats. Larger CH_4 emissions of up to ~75 nmol m^{-2} s^{-1} are observed near the St. Jones Reserve, a brackish herbaceous wetland, and up to ~180 nmol m^{-2} s^{-1} in the Alligator River Refuge, a freshwater woody wetland.

Our results also suggest that the tower sites located along the flight path capture ~30–75% of the regional variability in ecosystem-dependent fluxes of H, LE, and F_{CO2}, but the limited number of tower sites with F_{CH4} observations makes quantitative comparison difficult. Diversity in the underlying biophysical drivers of flux within land classes likely accounts for the observed regional-scale ecosystem variability. Moreover, the underlying biogeochemical controls of CH_4 flux in wetlands are often not directly tied to land class, including such factors as substrate availability, salinity, and water table depth. The persistently high CH_4 emissions observed during CARAFE at the local US-StJ and US-NC4 tower sites emphasize the need to further test the representativeness of these understudied and heterogeneous ecosystems.

Although towers offer limited regional representativeness both within and across ecosystem states, tower observations complement airborne EC by providing a long-term record of ecosystem-dependent carbon cycling. The tower sites in the CARAFE domain display nearly consistent relationships between peak- and daily-CO_2 exchange (within uncertainty), suggesting a means of upscaling to regional daily carbon cycle dynamics via airborne measurements.

While this study focused on thematic land cover, a wealth of remote sensing data yields unique opportunities to assess model-derived fluxes and quantify uncertainties in regional flux products. Potential future work includes extending the disaggregation methodology to derive relationships between observed fluxes and surface parameters such as canopy height, solar-induced chlorophyll fluorescence (SIF), or normalized difference vegetation index (NDVI) that initialize model- and satellite-derived fluxes (e.g. Hurtt *et al.*, 2004; Zhang *et al.*, 2014), thus enabling direct evaluation. Additionally, the spatially-distributed fluxes from airborne EC provide the unique capability of evaluating landscape-scale flux maps derived from remote sensing models (Anderson *et al.*, 2008) as well as gaining a greater understanding of boundary layer dynamics affecting flux footprint and source area modeling using large eddy simulations (Bertoldi *et al.*, 2013).

The importance of terrestrial ecosystems in the global CO_2 and CH_4 budgets motivates the need for continued measurements over regions where large uncertainties in carbon exchange persist, such as natural wetlands and areas of rapid environmental and land-use change. Incorporating remote-sensing surface information could further focus such studies, exploiting the full potential of airborne flux observations in constraining carbon cycle dynamics.

Acknowledgements

The CARAFE 2016 and 2017 missions were supported by the GSFC Internal Research and Development Program, the NASA Carbon Monitoring System Program (NNH15ZDA001N-CMS), and the NASA HQ Earth Science Division. We also acknowledge the following AmeriFlux sites for

their data records: US-Ced, US-NC4, US-Slt, and US-StJ. Funding for the AmeriFlux data resources was provided by the U.S. Department of Energy's Office of Science, and additional support for the US-StJ tower came from NSF grant #1652594. Research and flux data from US-Ced and US-Slt were supported by the Northern Research Station, USDA Forest Service. Data from the USDA-Agricultural Research Service is part of the Long-Term Agroecosystem Research (LTAR) program.

Data Availability

The data that support the findings of this study are openly available at the following DOIs: http://dx.doi.org/10.17190/AMF/1480314; http://dx.doi.org/10.17190/AMF/1246096; http://dx.doi.org/10.17190/AMF/1246043; http://dx.doi.org/10.17190/AMF/1480316; All data are available upon request from the corresponding author, and aircraft data can be publicly accessed: https://www-air.larc.nasa.gov/missions/carafe/index.html.

References

Abril, G. and Borges, A. V. (2005) 'Carbon dioxide and methane emissions from estuaries', in Tremblay, A. et al. (eds) *Greenhouse gas emissions – fluxes and processes*. Berlin, Heidleberg: Springer (Environmental Science), pp. 187–207.

Anderson, M. C. *et al.* (2008) 'A thermal-based remote sensing technique for routine mapping of land-surface carbon, water and energy fluxes from field to regional scales', *Remote Sensing of Environment*. Elsevier, 112(12), pp. 4227–4241.

Baldocchi, D. *et al.* (2001) 'FLUXNET: A new tool to study the temporal and spatial variability of ecosystem-scale carbon dioxide, water vapor, and energy flux densities', *Bulletin of the American Meteorological Society*. American Meteorological Society, 82(11), pp. 2415–2434.

Barrick, J. D. W. *et al.* (1996) *Calibration of NASA turbulent air motion measurement system*.

Bertoldi, G., Kustas, W. P. and Albertson, J. D. (2013) 'Evaluating source area contributions from aircraft flux measurements over heterogeneous land using large-eddy simulation', *Boundary-layer meteorology*. Springer, 147(2), pp. 261–279.

Bond-Lamberty, B. *et al.* (2018) 'Globally rising soil heterotrophic respiration over recent decades', *Nature*. Nature Publishing Group, 560(7716), p. 80.

Bousquet, P. *et al.* (2011) 'Source attribution of the changes in atmospheric methane for 2006--2008', *Atmospheric Chemistry and Physics*. Copernicus GmbH, 11(8), pp. 3689–3700.

Capooci, M. *et al.* (2019) 'Experimental influence of storm-surge salinity on soil greenhouse gas emissions from a tidal salt marsh', *Science of The Total Environment*. Elsevier, 686, pp. 1164–1172.

Chen, J. M. *et al.* (1999) 'Extending aircraft-and tower-based CO2 flux measurements to a boreal region using a Landsat thematic mapper land cover map', *Journal of Geophysical Research: Atmospheres*. Wiley Online Library, 104(D14), pp. 16859–16877.

Chevallier, F. *et al.* (2006) 'On the assignment of prior errors in Bayesian inversions of CO2 surface fluxes', *Geophysical Research Letters*. Wiley Online Library, 33(13).

Ciais, P. *et al.* (2013) 'Carbon and Other Biogeochemical Cycles', in *Climate Change 2013: The Physical Science Basis. Contribution of Working Group I to the Fifth Assessment Report of the Intergovernmental Panel on Climate Change*. Cambridge University Press, pp. 465–570.

Clark, K. *et al.* (2018) 'Decadal-scale reduction in forest net ecosystem production following insect defoliation contrasts with short-term impacts of prescribed fires', *Forests*. Multidisciplinary Digital Publishing Institute, 9(3), p. 145.

Cox, P. M. *et al.* (2013) 'Sensitivity of tropical carbon to climate change constrained by carbon dioxide variability', *Nature*. Nature Publishing Group, a division of Macmillan Publishers Limited. All Rights Reserved., 494, p. 341. Available at: https://doi.org/10.1038/nature11882.

Crawford, T. L. *et al.* (1996) 'Air-surface exchange measurement in heterogeneous regions: extending tower observations with spatial structure observed from small aircraft', *Global Change Biology*. Wiley Online Library, 2(3), pp. 275–285.

Desjardins, R. L. *et al.* (1982) 'Aircraft monitoring of surface carbon dioxide exchange', *Science*. American Association for the Advancement of Science, 216(4547), pp. 733–735.

Desjardins, R. L. *et al.* (1989) 'An evaluation of aircraft flux measurements of CO 2, water vapor and sensible heat', in *Boundary Layer Studies and Applications*. Springer, pp. 55–69.

Diskin, G. S. *et al.* (2002) 'Open-path airborne tunable diode laser hygrometer', in *Diode Lasers and Applications in Atmospheric Sensing*, pp. 196–205.

Dobosy, R. *et al.* (2017) 'Estimating random uncertainty in airborne flux measurements over Alaskan tundra: Update on the Flux Fragment Method', *Journal of Atmospheric and Oceanic Technology*, 34(8), pp. 1807–1822.

Frankenberg, C. *et al.* (2011) 'New global observations of the terrestrial carbon cycle from GOSAT: Patterns of plant fluorescence with gross primary productivity', *Geophysical Research Letters*. Wiley Online Library, 38(17).

Friend, A. D. *et al.* (2007) 'FLUXNET and modelling the global carbon cycle', *Global Change Biology*. Wiley Online Library, 13(3), pp. 610–633.

Gioli, B. *et al.* (2004) 'Comparison between tower and aircraft-based eddy covariance fluxes in five European regions', *Agricultural and Forest Meteorology*. Elsevier, 127(1–2), pp. 1–16.

Hayes, D. J. *et al.* (2018) 'Chapter 2: The North American carbon budget', in Cavallaro, N. et al. (eds) *Second State of the Carbon Cycle Report (SOCCR2): A Sustained Assessment Report*. Washington, DC: U.S. Global Change Research Program, pp. 71–108. doi: 10.7930/SOCCR2.2018.Ch2.

Hiller, R. V *et al.* (2014) 'Aircraft-based CH4 flux estimates for validation of emissions from an agriculturally dominated area in Switzerland', *Journal of Geophysical Research: Atmospheres*. Wiley Online Library, 119(8), pp. 4874–4887.

Horst, T. W. and Weil, Jc. (1992) 'Footprint estimation for scalar flux measurements in the atmospheric surface layer', *Boundary-Layer Meteorology*. Springer, 59(3), pp. 279–296.

Houghton, R. A. *et al.* (2012) 'Carbon emissions from land use and land-cover change', *Biogeosciences*. Copernicus GmbH, 9(12), pp. 5125–5142.

Houweling, S. *et al.* (2015) 'An intercomparison of inverse models for estimating sources and sinks of CO2 using GOSAT measurements', *Journal of Geophysical Research: Atmospheres*. Wiley Online Library, 120(10), pp. 5253–5266. doi: 10.1002/2014JD022962.

Huntzinger, D. N. *et al.* (2012) 'North American Carbon Program (NACP) regional interim synthesis: Terrestrial biospheric model intercomparison', *Ecological Modelling*. Elsevier, 232, pp. 144–157.

Hurtt, G. C. *et al.* (2004) 'Beyond potential vegetation: Combining lidar data and a height-structured model for carbon studies', *Ecological Applications*. Wiley Online Library, 14(3), pp. 873–883.

Hutjes, R. W. A. *et al.* (2010) 'Dis-aggregation of airborne flux measurements using footprint analysis', *Agricultural and Forest Meteorology*. doi: 10.1016/j.agrformet.2010.03.004.

Jung, M. *et al.* (2011) 'Global patterns of land-atmosphere fluxes of carbon dioxide, latent heat, and sensible heat derived from eddy covariance, satellite, and meteorological observations', *Journal of Geophysical Research: Biogeosciences*, 116(3), p. G00J07. doi: 10.1029/2010JG001566.

Kathilankal, J. C. *et al.* (2008) 'Tidal influences on carbon assimilation by a salt marsh', *Environmental Research Letters*. IOP Publishing, 3(4), p. 44010.

Kirby, S. *et al.* (2008) 'An aircraft-based data analysis method for discerning individual fluxes in a heterogeneous agricultural landscape', *Agricultural and Forest Meteorology*. Elsevier, 148(3), pp. 481–489.

Kljun, N. *et al.* (2015) 'A simple two-dimensional parameterisation for Flux Footprint Prediction

(FFP)', *Geoscientific Model Development*, 8(11), pp. 3695–3713. doi: 10.5194/gmd-8-3695-2015.

Kljun, N., Rotach, M. W. and Schmid, H. P. (2002) 'A three-dimensional backward Lagrangian footprint model for a wide range of boundary-layer stratifications', *Boundary-Layer Meteorology*. Springer, 103(2), pp. 205–226.

Kustas, W. P. *et al.* (2006) 'Using a remote sensing field experiment to investigate flux-footprint relations and flux sampling distributions for tower and aircraft-based observations', *Advances in Water Resources*. Elsevier, 29(2), pp. 355–368.

Lauvaux, T. *et al.* (2009) 'Bridging the gap between atmospheric concentrations and local ecosystem measurements', *Geophysical research letters*. Wiley Online Library, 36(19).

Leclerc, M. Y. and Thurtell, G. W. (1990) 'Footprint prediction of scalar fluxes using a Markovian analysis', *Boundary-Layer Meteorology*. Springer, 52(3), pp. 247–258.

Lenschow, D. H., Pearson Jr, R. and Stankov, B. B. (1981) 'Estimating the ozone budget in the boundary layer by use of aircraft measurements of ozone eddy flux and mean concentration', *Journal of Geophysical Research: Oceans*. Wiley Online Library, 86(C8), pp. 7291–7297.

Lokupitiya, E. *et al.* (2009) 'Incorporation of crop phenology in Simple Biosphere Model (SiBcrop) to improve land-atmosphere carbon exchanges from croplands', *Biogeosciences*. Copernicus GmbH, 6(6), pp. 969–986.

Maselli, F. *et al.* (2010) 'Validating an integrated strategy to model net land carbon exchange against aircraft flux measurements', *Remote Sensing of Environment*. Elsevier, 114(5), pp. 1108–1116.

Melton, J. R. *et al.* (2013) 'Present state of global wetland extent and wetland methane modelling: conclusions from a model inter-comparison project (WETCHIMP)', *Biogeosciences*, 10(2), pp. 753–788.

Metzger, S. *et al.* (2013) 'Spatially explicit regionalization of airborne flux measurements using environmental response functions', *Biogeosciences*. Copernicus GmbH, 10(4), p. 2193.

Miao, G. *et al.* (2017) 'Hydrology and microtopography control carbon dynamics in wetlands: Implications in partitioning ecosystem respiration in a coastal plain forested wetland', *Agricultural and forest meteorology*. Elsevier, 247, pp. 343–355.

Miglietta, F. *et al.* (2007) 'Net regional ecosystem CO 2 exchange from airborne and ground-based eddy covariance, land-use maps and weather observations', *Global Change Biology*, 13, pp. 548–560. doi: 10.1111/j.1365-2486.2006.01219.x.

Mitra, B., Noormets, A., *et al.* (2019) 'Coastal forested wetlands can be unquantified greenhouse gas emission hotspot', *Proceedings of the National Academy of Sciences*.

Mitra, B., Minick, K., *et al.* (2019) 'Spectral evidence for plant physiological and environmental control of methane emissions from a coastal forested wetland in North Carolina', *Agricultural and Forest Meteorology*.

Ogunjemiyo, S. O. *et al.* (2003) 'Methods of estimating CO2, latent heat and sensible heat fluxes from estimates of land cover fractions in the flux footprint', *Agricultural and Forest Meteorology*. Elsevier, 117(3), pp. 125–144.

Pacala, S. W. *et al.* (2001) 'Consistent Land- and Atmosphere-Based U.S. Carbon Sink Estimates', *Science*, 292(5525), pp. 2316–2320. doi: 10.1126/science.1057320.

Pan, Y. *et al.* (2011) 'A large and persistent carbon sink in the world's forests', *Science*. American Association for the Advancement of Science, 333(6045), pp. 988–993.

Poffenbarger, H. J., Needelman, B. A. and Megonigal, J. P. (2011) 'Salinity influence on methane emissions from tidal marshes', *Wetlands*. Springer, 31(5), pp. 831–842.

Le Quéré, C. *et al.* (2018) 'Global Carbon Budget 2018', *Earth System Science Data*, 10(4), pp. 2141–2194.

Raczka, B. M. *et al.* (2013) 'Evaluation of continental carbon cycle simulations with North American flux tower observations', *Ecological Monographs*. Wiley Online Library, 83(4), pp. 531–556.

Saunois, M. *et al.* (2016) 'The global methane budget 2000--2012', *Earth System Science Data*, 8(2), pp. 697–751.

Sayres, D. S. *et al.* (2017) 'Arctic regional methane fluxes by ecotope as derived using eddy covariance from a low-flying aircraft', *Atmospheric Chemistry and Physics*, 17, pp. 8619–8633.

Schaefer, K. *et al.* (2008) 'Combined simple biosphere/Carnegie-Ames-Stanford approach terrestrial carbon cycle model', *Journal of Geophysical Research: Biogeosciences*. Wiley Online Library, 113(G3).

Schaefer, K. *et al.* (2012) 'A model-data comparison of gross primary productivity: Results from the North American Carbon Program site synthesis', *Journal of Geophysical Research: Biogeosciences (2005–2012)*. Wiley Online Library, 117(G3). doi: 10.1029/2012JG001960.

Schmid, H. P. (1994) 'Source areas for scalars and scalar fluxes', *Boundary-Layer Meteorology*. Springer, 67(3), pp. 293–318.

Schuepp, P. H. *et al.* (1990) 'Footprint prediction of scalar fluxes from analytical solutions of the diffusion equation', *Boundary-Layer Meteorology*. Springer, 50(1–4), pp. 355–373.

Schwalm, C. R. *et al.* (2010) 'A model-data intercomparison of CO2 exchange across North America: Results from the North American Carbon Program site synthesis', *Journal of*

Geophysical Research: Biogeosciences. Wiley Online Library, 115(G3).

Sellers, P. J. *et al.* (1997) 'BOREAS in 1997: Experiment overview, scientific results, and future directions', *Journal of Geophysical Research: Atmospheres*. Wiley Online Library, 102(D24), pp. 28731–28769.

Subke, J.-A. *et al.* (2018) 'Rhizosphere activity and atmospheric methane concentrations drive variations of methane fluxes in a temperate forest soil', *Soil Biology and Biochemistry*. Elsevier, 116, pp. 323–332.

Sun, L. *et al.* (2017) 'Investigating water use over the Choptank River Watershed using a multisatellite data fusion approach', *Water Resources Research*. Wiley Online Library, 53(7), pp. 5298–5319.

Thornhill, K. L. *et al.* (2003) 'Air motion intercomparison flights during Transport and Chemical Evolution in the Pacific (TRACE-P)/ACE-ASIA', *Journal of Geophysical Research: Atmospheres*. Wiley Online Library, 108(D20).

Tian, H. *et al.* (2016) 'The terrestrial biosphere as a net source of greenhouse gases to the atmosphere', *Nature*. Nature Publishing Group, a division of Macmillan Publishers Limited. All Rights Reserved., 531, p. 225. Available at: https://doi.org/10.1038/nature16946.

Torrence, C. and Compo, G. P. (1998) 'A practical guide to wavelet analysis', *Bulletin of the American Meteorological society*. American Meteorological Society, 79(1), pp. 61–78.

Turetsky, M. R. *et al.* (2014) 'A synthesis of methane emissions from 71 northern, temperate, and subtropical wetlands', *Global change biology*. Wiley Online Library, 20(7), pp. 2183–2197.

Turner, A. J., Frankenberg, C. and Kort, E. A. (2019) 'Interpreting contemporary trends in atmospheric methane', *Proceedings of the National Academy of Sciences*. National Academy of Sciences, p. 201814297.

Vargas, R. and Barba, J. (2019) 'Greenhouse gas fluxes from tree stems', *Trends in plant science*. Elsevier, 24(4), pp. 296–299.

Villarreal, S. *et al.* (2018) 'Ecosystem functional diversity and the representativeness of environmental networks across the conterminous United States', *Agricultural and forest meteorology*. Elsevier, 262, pp. 423–433.

Wang, J. S. *et al.* (2018) 'A global synthesis inversion analysis of recent variability in CO2 fluxes using GOSAT and in situ observations', *Atmospheric Chemistry and Physics*. Copernicus GmbH, 18(15), pp. 11097–11124.

Wang, W. *et al.* (2006) 'Decomposing CO2 fluxes measured over a mixed ecosystem at a tall tower and extending to a region: A case study', *Journal of Geophysical Research: Biogeosciences*. Wiley Online Library, 111(G2).

Wenzel, S. *et al.* (2016) 'Projected land photosynthesis constrained by changes in the seasonal cycle of atmospheric CO2', *Nature*. Macmillan Publishers Limited, part of Springer Nature. All rights reserved., 538, p. 499. Available at: https://doi.org/10.1038/nature19772.

Whalen, S. C. (2005) 'Biogeochemistry of Methane Exchange between Natural Wetlands and the Atmosphere', *Environmental Engineering Science*, 22(1), pp. 73–94. doi: 10.1089/ees.2005.22.73.

Wolfe, G. M. *et al.* (2018) 'The NASA Carbon Airborne Flux Experiment (CARAFE): instrumentation and methodology', *Atmospheric Measurement Techniques*, 11(3), pp. 1757–1776. doi: 10.5194/amt-11-1757-2018.

Yang, L. *et al.* (2018) 'A new generation of the United States National Land Cover Database: Requirements, research priorities, design, and implementation strategies', *ISPRS Journal of Photogrammetry and Remote Sensing*. Elsevier, 146, pp. 108–123.

Zhang, X. *et al.* (2015) 'Regional scale cropland carbon budgets: Evaluating a geospatial agricultural modeling system using inventory data', *Environmental Modelling & Software*, 63, pp. 199–216. doi: https://doi.org/10.1016/j.envsoft.2014.10.005.

Zhang, Y. *et al.* (2014) 'Estimation of vegetation photosynthetic capacity from space-based measurements of chlorophyll fluorescence for terrestrial biosphere models', *Global Change Biology*, 20(12), pp. 3727–3742. doi: 10.1111/gcb.12664.

Zscheischler, J. *et al.* (2016) 'Short-term favorable weather conditions are an important control of interannual variability in carbon and water fluxes', *Journal of Geophysical Research: Biogeosciences*. Wiley Online Library, 121(8), pp. 2186–2198.

Zulueta, R. C. *et al.* (2013) 'Aircraft regional-scale flux measurements over complex landscapes of mangroves, desert, and marine ecosystems of Magdalena Bay, Mexico', *Journal of Atmospheric and Oceanic Technology*, 30(7), pp. 1266–1294.

Table 1. Summary of flux towers underlying CARAFE flight tracks. The primary NLCD 2016 land class is also listed.

Tower	Description	Lat, Long	Land Class	Measurements	Overfly Date
US-Ced	Cedar Bridge, NJ	39.8379° N 74.3791° W	Evergreen forest	H, LE, F_{CO2}	20160914 20160923 20170509
US-Slt	Silas Little, NJ	39.9138° N 74.5960° W	Deciduous forest	H, LE, F_{CO2}	20160914 20160923 20170509
US-NC4	Alligator River, NC	35.7879° N 75.9038° W	Woody wetlands	H, LE, F_{CO2} F_{CH4}	20160924 20170515 20170526
US-StJ	St. Jones, DE	39.0882° N 75.4372° W	Herbaceous wetlands	H, LE, F_{CO2} F_{CH4}	20160912 20170504 20170518
USDA-Chop	Choptank, MD	39.0587° N 75.8513° W	Cultivated crops	H, LE, F_{CO2}	20160912 20170504 20170518

Table 2. Summary of land cover contributions for Choptank/St.Jones and Alligator River case studies. FP-weighted area is the mean for all flights.

Region	Land Class	FP-Area
Choptank/St. Jones	Cultivated crops	56%
	Woody wetlands	21%
	Deciduous forest	6%
	Developed-Open	6%
	Herbaceous wetlands	<5%
	Open water	<5%
Alligator River	Woody wetlands	83%
	Open water	10%
	Cultivated crops	<5%
	Herbaceous wetlands	<5%

Table 3. Linear regression parameters for daily NEE vs. peak-NEE both in units of µmol m^{-2} s^{-1} calculated using the flux tower observations from 2016. Slope and intercept are listed with 95% confidence intervals.

Tower	Slope	Intercept	r^2	RMSE‡
US-Ced	0.31 ± 0.02	-0.64 ± 0.16	0.78	0.90
US-Slt	0.30 ± 0.02	-0.84 ± 0.15	0.81	1.04
US-NC4	0.30 ± 0.02	-0.44 ± 0.11	0.83	0.73
US-StJ	0.21 ± 0.02	-1.10 ± 0.30	0.54	1.95
USDA-Chop	0.27 ± 0.01	-0.36 ± 0.12	0.88	0.89

‡Units: µmol m^{-2} s^{-2}

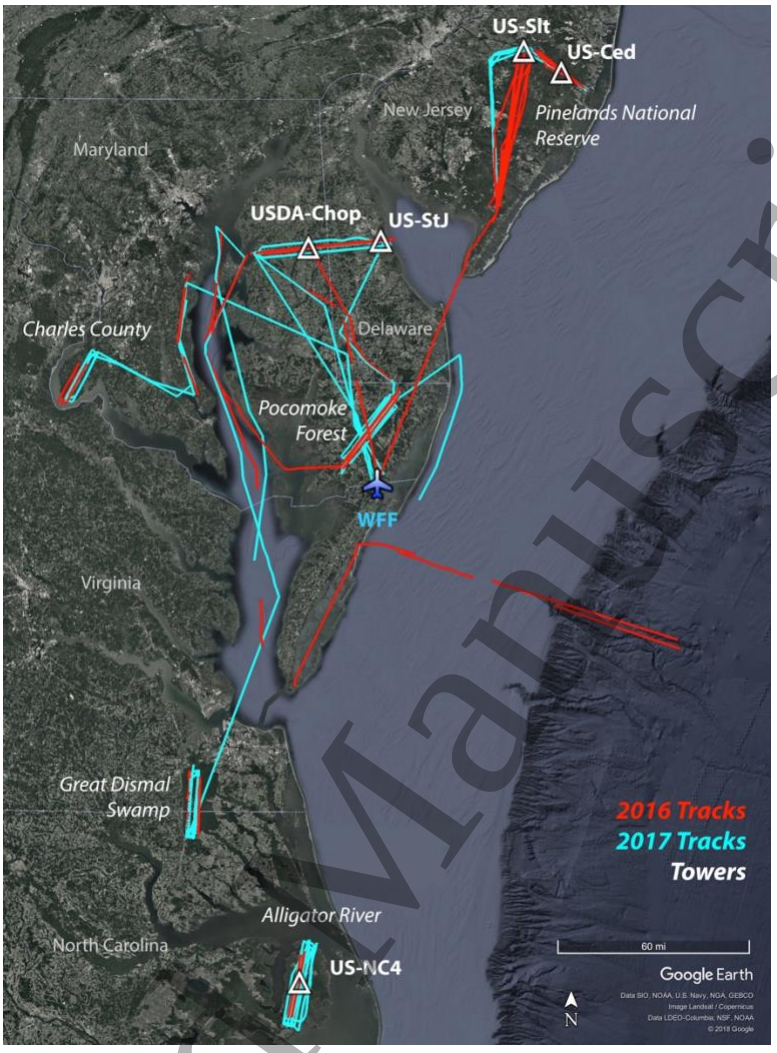

Figure 1. Map of the NASA CARAFE flux transects from September 2016 (red) and May 2017 (cyan). All flights were based out of Wallops Flight Facility (WFF) in Wallops, VA. The locations of five flux towers situated beneath the flight tracks are indicated by white triangles.

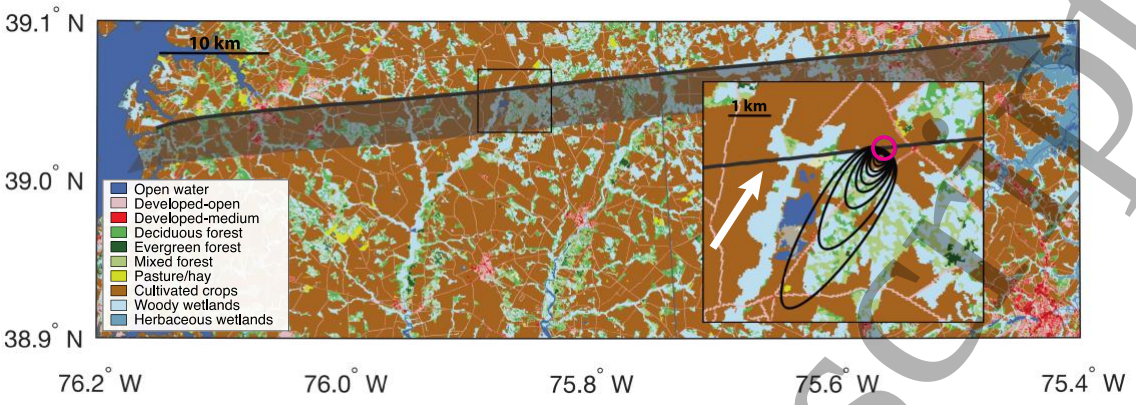

Figure 2. A single flux transect from the May 18, 2017 flight over the Choptank/St. Jones region, overlaid on the NLCD 2016 land cover map. The grey shading indicates the cumulative footprint for all observation points along the leg. The inset box shows a single 2D footprint calculated using the Kljun et al. (2015) parameterization, with black contours depicting weighted contributions to the observed flux from 10–90% in 10% increments. The white arrow denotes the mean horizontal wind direction, and the magenta circle indicates the 200 m radius around the USDA-Choptank tower.

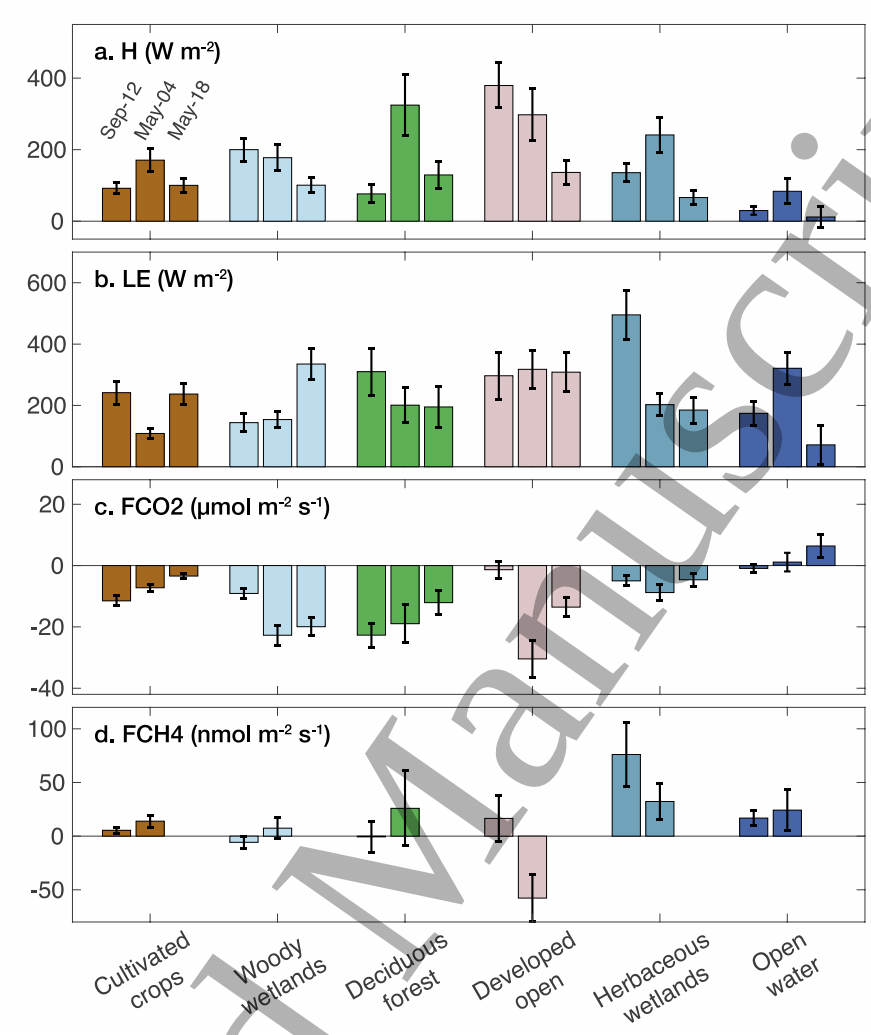

Figure 3. Disaggregated fluxes by land class for flights to the Choptank Watershed region: (a) Sensible heat flux; (b) latent heat flux; (c) CO_2 flux; and (d) CH_4 flux. Land class fluxes are grouped by fractional area and ordered by flight date from left to right. Note that September dates are from the 2016 campaign and May dates are from 2017. Error bars represent ±2σ uncertainty in the component flux, which includes systematic and random error propagated through the regression analysis, in addition to the regression residuals. CARAFE was not sampling fast CH_4 measurements on May-18, and no F_{CH4} data are available on this date.

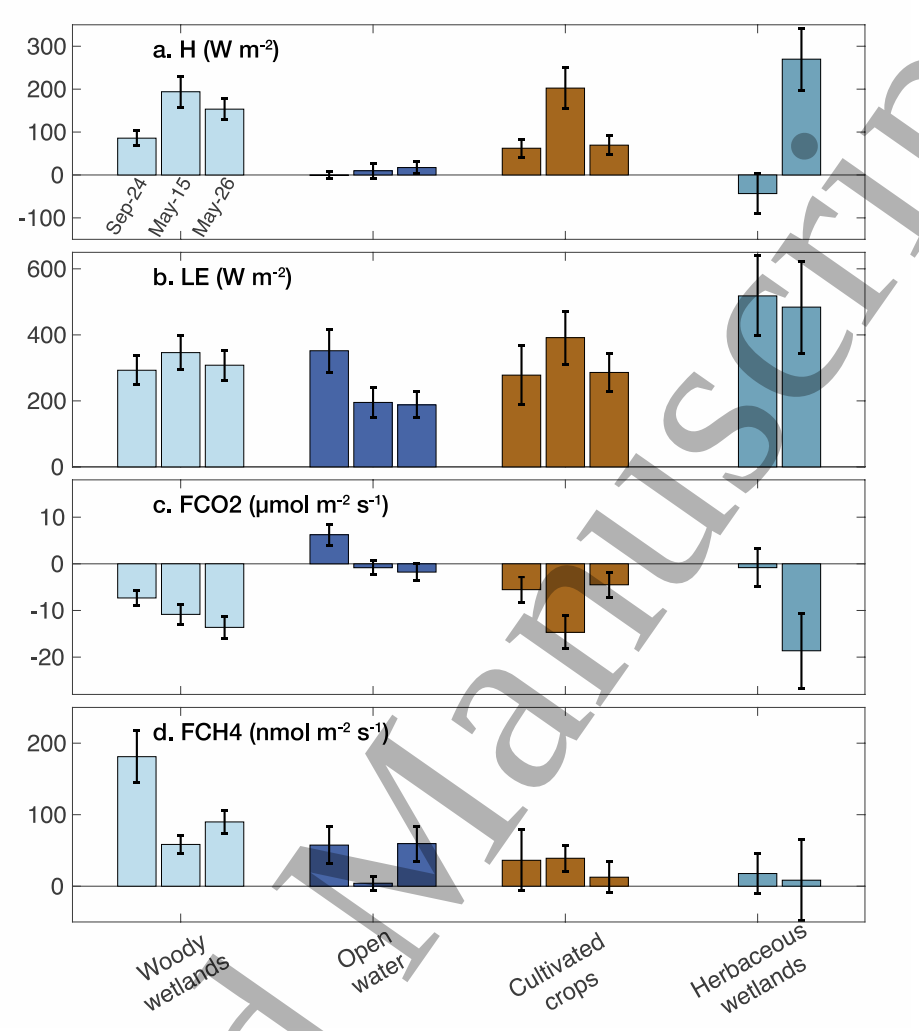

Figure 4. As in Fig. 3, but for flights to the Alligator River in North Carolina. Emergent wetlands were not sufficiently represented in the Sep-24 observation footprints.

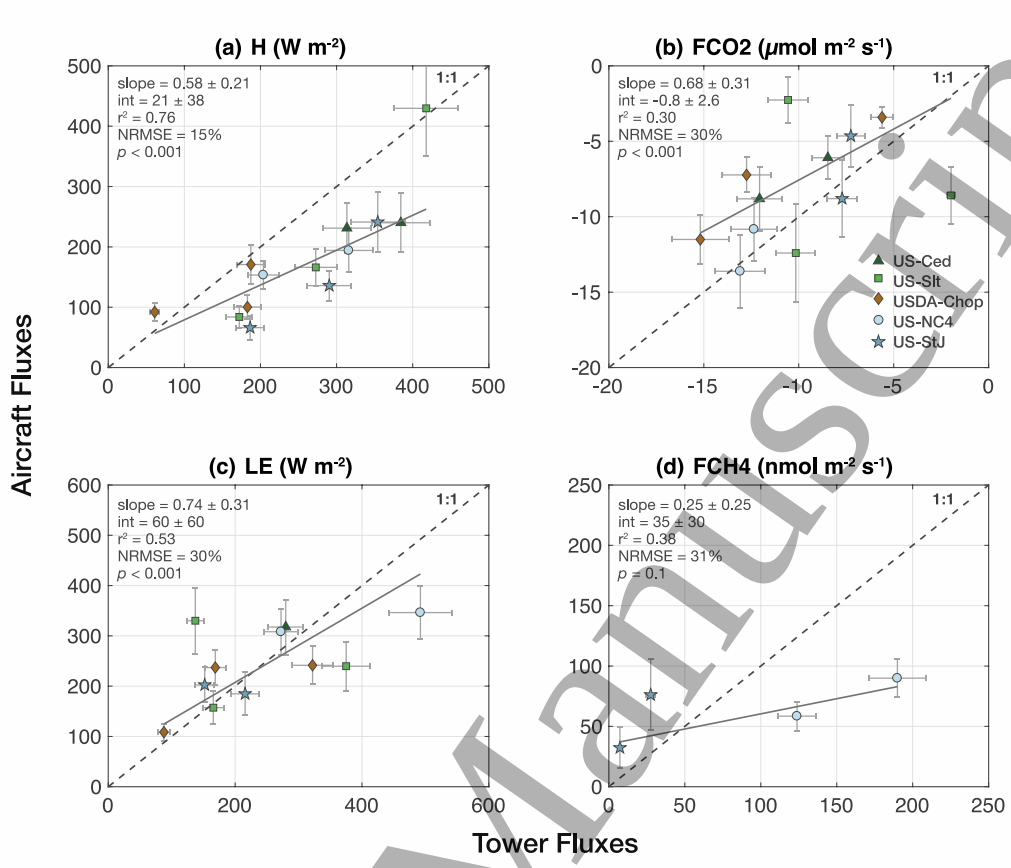

Figure 5. Comparison of disaggregated aircraft fluxes and tower fluxes by land class for (a) sensible heat, (b) CO_2, (c) latent heat, and (d) CH_4. Error bars for aircraft observations indicate $\pm 2\sigma$ uncertainty, which includes systematic and random error propagated through the regression analysis, in addition to the regression residuals. Tower errors are assumed to be ± 10%. The dashed line is the 1:1 reference, and the solid grey line indicates the best fit, with slope and intercept reported with 95% confidence intervals. The towers sample the following land classes: Evergreen forest (US-CED), deciduous forest (US-Slt), cultivated crops (USDA-Chop), woody wetlands (US-NC4), and herbaceous wetlands (US-StJ).

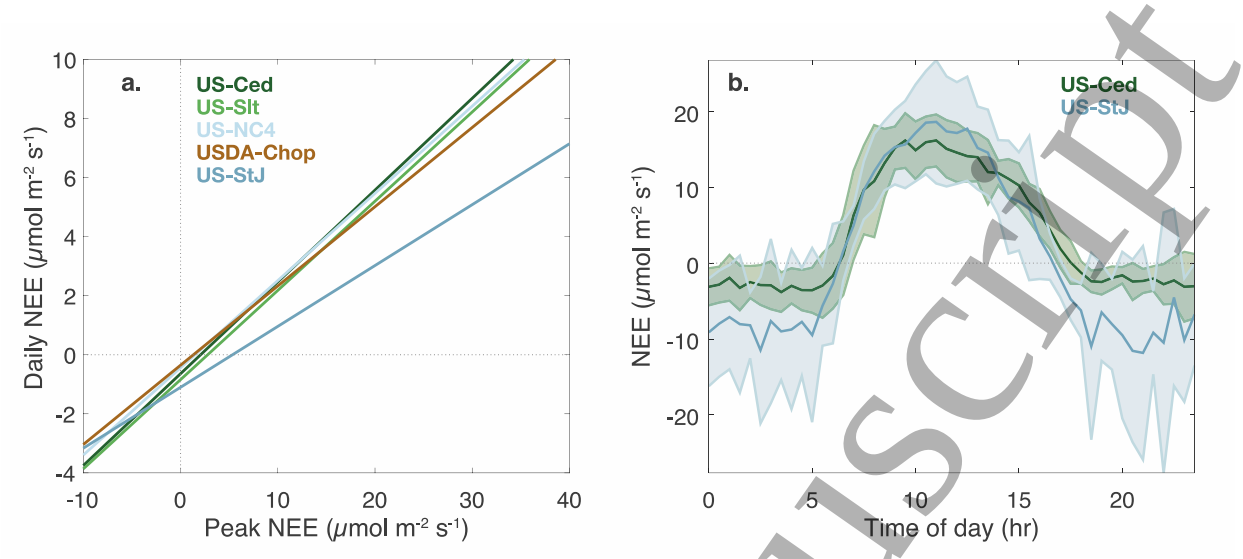

Figure 6. Linear fits of the daily NEE vs. peak NEE for the five tower sites in 2016 (a). The fits are colored by the tower land class: US-Ced (deciduous forest), US-Slt (mixed forest), US-NC4 (woody wetland), USDA (cultivated crops), US-StJ (herbaceous wetlands). Monthly mean diurnal CO_2 fluxes for US-Ced and US-StJ during August 2016 (b). The shaded area indicates the $\pm 1\sigma$ of all NEE observations over the given timeframe.